General approach to spatiotemporal modulational instability processes

P. Béjot,* B. Kibler, E. Hertz, B. Lavorel, and O. Faucher

Laboratoire Interdisciplinaire Carnot de Bourgogne, Unité Mixte de Recherche 5209, Centre National de la Recherche Scientifique–Université de Bourgogne, BP 47870, F-21078 Dijon CEDEX, France

(Received 21 September 2010; published 31 January 2011)

In this article, we derive the general exact solution of the modulation instability gain. The solution described here is valid for 1-D, 2-D, and 3-D cases considering any temporal response function of the medium and with possible higher order Kerr nonlinearities. In particular, we show that the gain induced by modulation instability is initial condition dependent, while the usual calculations do not lead to such a dependence. Applications for current and high-interest nonlinear propagation problems, such as 1-D optical fiber propagation with delayed Raman response and 2-D filamentation in gases, are investigated in detail. More specifically, we demonstrate that the 2-D model of filamentation based on the balance between higher order Kerr terms leads to a modulation instability window. The impact of both self-steepening and space-time defocusing effects is also highlighted. Finally, we discuss the influence of the finite-time response of the different order electronic Kerr effects on the growth of the expected modulation instability bands.

DOI: 10.1103/PhysRevA.83.013830 PACS number(s): 42.65.Ky, 42.65.Sf, 42.81.Dp

I. INTRODUCTION

From the 1960s until today, the modulation instability (MI) process has remained the subject of numerous experimental and numerical studies in transparent materials [1–6]. When a quasicontinuous wave propagates through a nonlinear medium, it can experience, in appropriate phase-matching conditions, spatiotemporal instabilities that manifest themselves by the exponential growth of weak perturbations. More specifically, MI results from the interplay between linear effects, such as group-velocity dispersion (GVD) or diffraction, and the Kerr-induced nonlinearity. For instance, in optical waveguides, if the focusing (defocusing) nonlinear medium exhibits anomalous (normal) dispersion at the pump frequency ω_0, because processes such as $\omega_0+\omega_0\rightarrow(\omega_0+\omega)+(\omega_0-\omega)$ can be nonlinearly phase matched, spectral bands spontaneously grow symmetrically with respect to the input wave frequency even in the absence of any seed. However, both higher order dispersion and birefringence characteristics can strongly affect the existence of new windows of scalar and vectorial MI effects [7,8]. Similarly, MI can also appear in the spatial domain because of the balance between diffraction and the Kerr effect. For instance, it has been shown that multifilamentation [9], that is, the splitting of an ultrashort ultra-high-power laser into several distinct structures, is a direct manifestation of spatial MI. On the other hand, recent experiments have been able to determine the higher nonlinear refractive indices of gases such as argon, nitrogen, and oxygen [10]. These higher nonlinear indices manifest themselves at high intensity by the cancellation and even a sign reversal of the global nonlinear refractive index of the considered gases. These measurements are of particular importance for the understanding of pulse propagation dynamics since it has been demonstrated that in some conditions, these indices are responsible for the collapse saturation during the filamentation process [11]. The scope of this article is then twofold. In Sec. II, we theoretically study the stability of the nonlinear Schrödinger equation and derive the exact solution for MI. This solution is valid for 1-D, 2-D, and 3-D propagation cases and is established with potential higher order Kerr terms and noninstantaneous temporal responses. The master equation derived here can hence describe any situation of scalar MI. Moreover, conversely to usual derivation of MI gain, we show that the gain bands are strongly dependent on the initial noise conditions. In Sec. III, we apply this analytical basis to investigate in detail the MI process for different configurations and materials. First, according to the recent measurements of higher order Kerr terms of some gases, we demonstrate the existence of a 2-D MI regime directly induced by these nonlinear indices. Indeed, on-axis MI can occur in the normal dispersion regime when the global nonlinear refractive index becomes negative at very high intensities. Moreover, we analyze how the self-steepening and space-time defocusing terms modify the MI bands. Second, we show that the master equation gives also the exact solution of MI in optical fibers when a delayed Raman effect is taken into account. In particular, we predict possible complex configurations of MI gain bands using the widely used waveguide category of photonic crystal fibers. Finally, we study the influence of the electronic finite-time response on the MI. In particular, we demonstrate that the time response of the Kerr-induced nonlinear index has to be relevantly evaluated in order to accurately describe MI band growth.

II. MODULATIONAL INSTABILITY ANALYSIS

In this section, we consider a linearly polarized (along a vector $\mathbf{u}$) electric field propagating in a transparent centrosymmetric medium. The electric field can be written as

$$\mathbf{E}(\overrightarrow{r},z,t)=[\varepsilon(\overrightarrow{r},z,t)e^{ik_0z-i\omega_0t}+\text{c.c.}]\mathbf{u}, \tag{1}$$

where c.c. denotes complex conjugation, ε is the slowly varying envelope, $\overrightarrow{r}$ is the transverse direction, and k_0 is the wave vector at the associated pulsation ω_0.

*pierre.bejot@u-bourgogne.fr

 ©2011 American Physical Society

In the frame propagating at the pump frequency group velocity $v_g = 1/k^{(1)}$ and neglecting harmonic generation, ε verifies

$$\partial_z \varepsilon = \frac{i}{2k_0} T^{-1} \triangle_\perp \varepsilon + i \sum_{n \geqslant 2} \frac{k^{(n)}}{n!} (i\partial_t)^n \varepsilon + i T k_0 \Delta n \varepsilon, \quad (2)$$

where $k^{(n)} = (\partial^n k)/(\partial \omega^n)|_{\omega_0}$ is the nth-order dispersion coefficient of the medium evaluated at ω_0 and Δn is the nonlinear refractive index. $\triangle_\perp = \partial^2/\partial x^2 + \partial^2/\partial y^2$ in 3-D or $\triangle_\perp = \partial^2/\partial r^2 + 1/r(\partial/\partial r)$ in 2-D denotes the transverse Laplacian. Assuming that the medium is transparent, Δn can be written as $\Delta n = \sum_{j \geqslant 1} n_{2j} R_{2j}(t) \star |\varepsilon|^{2j}$, where $\star$ accounts for convolution [12]. Depending on the considered medium, one can consider only n_2 (e.g., for propagation in fiber) or a full development up to n_{10} (as shown in [11]). $R_{2j}(t)$ accounts for the $(2j+1)$th-order temporal response function of the medium, which are all real and verify $\int_{-\infty}^{\infty} R_{2j}(t)dt = 1$ and $R_{2j}(t<0) = 0$. $R_2(t)$ can take into account both electronic induced nonlinear responses (generally admitted as instantaneous) and vibrational or rotational responses. For instance, for silica fiber-propagation problems, one generally takes $R_2(t) = (1-f_r)\delta(t) + f_r H(t)$ with $H(t) = f_a h_a(t) + f_b h_b(t)$, where δ is the Dirac function; $h_a = \tau_1(\tau_1^{-2} + \tau_2^{-2}) e^{-t/\tau_2} \sin(t/\tau_1)$; $h_b = \frac{2\tau_b - t}{\tau_b} e^{-t/\tau_b}$; $f_r = 0.18$; $f_a = 0.79$; $f_b = 0.21$; $\tau_1 = 12.2$ fs; $\tau_2 = 32$ fs; $\tau_b = 96$ fs; and n_{2j} $(j>1) = 0$ [13]. In the air propagation problem, one takes $R_2(t) = (1-f_r)\delta(t) + f_r H(t)$, where $H(t) = \tau_1(\tau_1^{-2} + \tau_2^{-2}) e^{-t/\tau_2} \sin(t/\tau_1)$; $f_r = 0.5$; $\tau_1 = 62.5$ fs; and $\tau_2 = 70$ fs, with the higher order nonlinear indices n_{2j} measured recently in [10]. In both cases, the electronic nonlinear response is considered as instantaneous. Finally, $T = 1 + (ik^{(1)})/(k_0)\partial_t$ $[T^{-1} = 1 - (ik^{(1)}/k_0)\partial_t]$ accounts for self-steepening (space-time defocusing). Equation (2) allows us to describe the propagation of electric field up to the single-cycle limit [14].

The steady state solution (i.e., considering a monochromatic plane wave) of Eq. (2) can be expressed as

$$\varepsilon(z) = \sqrt{I_0} e^{i k_0 D_n z}, \quad (3)$$

with $D_n = \sum_{j \geqslant 1} n_{2j} I_0^j$ and I_0 being the incident intensity.

The stability of the continuous-wave steady state solution of Eq. (2) is examined by studying the evolution of the system in the presence of a small complex perturbation $a(r,t)$:

$$\varepsilon(z) = [\sqrt{I_0} + a(r,t)] e^{i k_0 D_n z}, \quad (4)$$

with $|a(r,t)|^2 \ll I_0$. Substituting Eq. (4) into Eq. (2) and linearizing, we find the equation describing the evolution of $a(r,t)$:

$$\partial_z a(r,t) = T^{-1} \frac{i}{2k_0} \triangle_\perp a(r,t) + i \left(\sum_{n \geqslant 2} \frac{k^{(n)}}{n!} (i\partial_t)^n \right) a(r,t) + i T k_0 I_0 n_{2_{\text{eff}}}(t) \star [a(r,t) + a^*(r,t)],$$

where

$$n_{2_{\text{eff}}}(t) = \sum_{j \geqslant 1} j R_{2j}(t) n_{2j} I_0^{j-1}. \quad (5)$$

If one considers a cylindrical symmetry around the propagation axis and considering that $a(r,t) = \mathcal{H}(\int_{-\infty}^{\infty} \widetilde{a}(k_\perp,\omega) e^{-i\omega t} d\omega)$, where $\mathcal{H}$ is the Hankel transform defined as $\mathcal{H}(f)(r) = \int_0^\infty k_\perp J_0(k_\perp r) f(k_\perp) dk_\perp$ with J_0 being the zeroth-order Bessel function, one obtains the propagation equation for $\widetilde{a}(k_\perp,\omega)$:

$$\partial_z \widetilde{a}(k_\perp,\omega) = -i \left[\frac{k_\perp^2}{2k_0} \left(1 - \frac{k^{(1)}}{k_0}\omega \right) - \sum_{n \geqslant 2} \frac{k^{(n)}}{n!} \omega^n \right] \widetilde{a}(k_\perp,\omega) + i k_0 \left(1 + \frac{k^{(1)}}{k_0}\omega \right) I_0 n_{2_{\text{eff}}}(\omega) [\widetilde{a}(k_\perp,\omega) + \widetilde{a}^*(-k_\perp,-\omega)], \quad (6)$$

where $n_{2_{\text{eff}}}(\omega) = \int_{-\infty}^{\infty} n_{2_{\text{eff}}}(t) e^{i\omega t} dt$.

Writing the equation propagation for $\widetilde{a}^*(-k_\perp,-\omega)$, using the fact that $n_{2_{\text{eff}}}(\omega) = n_{2_{\text{eff}}}^*(-\omega)$ [since all $R_{2j}(t)$ are real], and defining $u = \widetilde{a}(k_\perp,\omega) + \widetilde{a}^*(-k_\perp,-\omega)$ and $v = \widetilde{a}(k_\perp,\omega) - \widetilde{a}^*(-k_\perp,-\omega)$, u and v then satisfy the following partial differential equation system:

$$\begin{aligned} \frac{\partial u}{\partial z} &= i[D_- u + (D_+ + S) v], \\ \frac{\partial v}{\partial z} &= i[(D_+ + N) u + D_- v], \end{aligned} \quad (7)$$

where

$$D_+ = -\frac{k_\perp^2}{2k_0} + \sum_{n \geqslant 1} \frac{k^{(2n)}}{(2n)!} \omega^{2n},$$
$$N = 2k_0 I_0 n_{2_{\text{eff}}}(\omega),$$
$$D_- = \frac{k_\perp^2 k^{(1)}}{2k_0^2}\omega + \sum_{n \geqslant 1} \frac{k^{(2n+1)}}{(2n+1)!} \omega^{2n+1},$$
$$S = 2k^{(1)} \omega I_0 n_{2_{\text{eff}}}.$$

Defining $K = \sqrt{-D_+(D_+ + N) - (S^2/4)}$ and $\Phi(z) = (D_- + S/2)z$, the two solutions of Eq. (7) are

$$u(z) = \frac{e^{i\Phi(z)}}{2} \times \left(u_0 \cosh(Kz) + i \frac{D_+ v_0 + \frac{S}{2} u_0}{K} \sinh(Kz) \right)$$

$$v(z) = \frac{e^{i\Phi(z)}}{2} \times \left(v_0 \cosh(Kz) + i \frac{(D_+ + N) u_0 - \frac{S}{2} v_0}{K} \sinh(Kz) \right),$$

where $u_0(k_\perp,\omega) = u(k_\perp,\omega,z=0)$ and $v_0(k_\perp,\omega) = v(k_\perp,\omega,z=0)$. Finally, the evolution of the perturbation $\widetilde{a}(k_\perp,\omega)$ can be expressed as

$$\widetilde{a}(k_\perp,\omega) = e^{i\Phi(z)} \left(\widetilde{a}_0 \cosh(Kz) + i \frac{\widetilde{A}_0}{K} \sinh(Kz) \right), \quad (8)$$

where $\widetilde{A}_0 = [D_+ \widetilde{a}_0 + N/2(\widetilde{a}_0 + \widetilde{a}_0{}^\sharp) + (S/2)\widetilde{a}_0{}^\sharp]$, with $\widetilde{a}_0 = \widetilde{a}(k_\perp,\omega,z=0)$ and $\widetilde{a}_0{}^\sharp = \widetilde{a}^*(-k_\perp,-\omega,z=0)$. In the following numerical simulations, $\widetilde{a}_0$ is the initial noise spectrum calculated as $\widetilde{a}_0 = \mathcal{H}(\int_{-\infty}^{\infty} a(r,t,z=0) e^{i\omega t} dt)$, while $\widetilde{a}_0{}^\sharp$ is calculated as $\widetilde{a}_0{}^\sharp = \mathcal{H}(\int_{-\infty}^{\infty} a^*(r,t,z=0) e^{i\omega t} dt)$.

The evolution of the spatiotemporal noise is then governed by Eq. (8). In particular, MI occurs when $\mathrm{Re}(K) > 0$, that is, when $D_+(D_+ + N) + S^2/4 < 0$, roughly leading to an exponential growth of a. More precisely, MI occurs if $(-N - \sqrt{N^2 - S^2})/(2) < D_+ < (-N + \sqrt{N^2 - S^2})/(2)$. Equation (8) is a general solution of MI in any nonlinear medium which can present a delayed nonlinear response and higher order nonlinear Kerr terms. However, one has to emphasize that this equation can be extended to a 3-D model by replacing $k_\perp^2$ by $k_x^2 + k_y^2$ and considering a 2-D spatial Fourier transform instead of a Hankel transform. Moreover, the 1-D case (i.e., for fiber-propagation issues) is obtained by setting $k_\perp = 0$. One generally uses an ansatz function for a [8,15–19]. Using such a method does not allow us to retrieve the exact solution for the evolution of a. Instead, one can only evaluate a gain (which does not intrinsically depend on the initial seeding). The fact that the growth is dependent on the initial noise could play a role in rogue wave generation [20]. Moreover, considering the initial condition dependence of Eq. (8) at a fixed ω, the maximal gain is dependent on the spatial gradient of both $\widetilde{a}_0$ and $\widetilde{a}_0{}^\sharp$. Consequently, it explains why multifilamentation occurs in the region of strong noise gradients. Since we have neglected the nonlinear terms with respect to a, the only limit of validity of this model is potential cascading phenomena, which can occur when $|a|^2$ becomes nonnegligible.

III. RESULTS AND DISCUSSION

A. 2-D analysis

In this section, we consider the propagation in argon of a cylindrical pump beam in order to investigate the impact of its higher order Kerr coefficients, which have been recently measured up to n_{10} [10]. Moreover, we assume here that all the nonlinear responses are instantaneous, that is, $R_{2j}(t) = \delta(t)\,\forall j$. Figure 1 shows the comparison between the integration of Eq. (2) and the results obtained from Eq. (8) for two different regimes in argon at atmospheric pressure and in a normal dispersion regime. As demonstrated in [11], Eq. (2) can accurately describe the propagation of filaments, providing that the plasma contribution stays negligible. The numerical simulations were performed by starting from a CW pump with a superimposed small noise (with a random spectral phase added to each frequency bin) as a seed for the MI. Since, in real experiments, the perturbations have their maximum intensity at the laser central frequency, in the frequency domain, and at the center of the pulse, in the spatial domain, we have also checked that using a noise with an amplitude presenting a Gaussian distribution centered on the pump frequency in both spectral and spatial domains does not affect qualitatively the MI bands. We clearly note the excellent quantitative agreement between analytical and numerical results, thus confirming the validity of our calculations. It is worth mentioning that calculations using an ansatz would only allow us to retrieve the envelope of the gain but not its fine structure.

Figure 1(a) [Fig. 1(b)] displays the analytical (numerical) MI gain bands for a 20 TW/cm^2 pump propagating through 1 m of argon at atmospheric pressure. At low intensities ($n_{2_{\mathrm{eff}}} > 0$), the gain displays an X pattern in the $(k_\perp, \omega)$ space. Neglecting higher order dispersion coefficients,

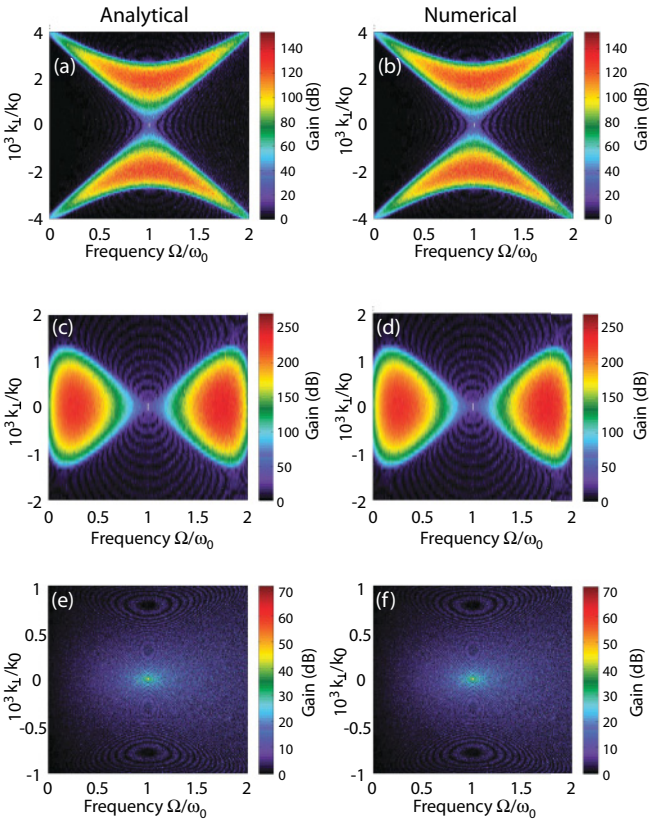

FIG. 1. (Color online) (left) Analytical and (right) numerical MI gain (dB) after propagation of a (top) 20 TW/cm^2, (middle) 30 TW/cm^2, and (bottom) 40 TW/cm^2 pump trough 1 m in argon when taking into account both self-steepening and space-time defocusing.

four-wave mixing processes $\omega_0 + \omega_0 \to (\omega_0 + \omega) + (\omega_0 - \omega)$ are phase matched if the condition $(N - \sqrt{N^2 - S^2})/(2) \leqslant (k_\perp^2)/(2k_0) - k^{(2)}\omega^2 \leqslant (N + \sqrt{N^2 - S^2})/(2)$ is respected. At the pump frequency ($\omega = 0$) and considering the temporal response of the medium as instantaneous, instabilities are maximal for $k_{\perp_{\max}}^2 = 2k_0^2 I_0 n_{2_{\mathrm{eff}}}$. This instability can then lead to the pulse breakup and consequently to multifilamentation. Moreover, one can associate with this instability a power $P = \pi I_0/k_{\perp_{\max}}^2 = \lambda_0^2/(8\pi n_{2_{\mathrm{eff}}})$ which corresponds to the widely studied critical power. Neglecting the higher order Kerr terms, if a pulse carries a power above P, then it will lead to a self-similar blowup singularity of Eq. (2) and to the pulse collapse [1].

For other frequencies, instabilities are maximal for $k_{\perp_{\max}}^2 = 2k_0\{\sum_{n\geqslant 1}(k^{(2n)})/[(2n)!]\omega^{2n} + k_0 I_0 n_{2_{\mathrm{eff}}}\}$. Figure 2 compares the emission angle $\theta(\omega) = k_{\perp_{\max}}/k(\omega)$ obtained with our calculations for $I_0 = 20$ TW/cm^2 (an offset corresponding to the natural divergence of a pulse with a waist of 200 μm has been added) with those experimentally measured in the visible [21] and in the infrared [22]. Even if MI calculations are intrinsically done with a continuous plane wave with an infinite spatial extension (which does not correspond to filamentation of ultrashort pulses), MI calculations accurately reproduce the conical emission induced during the filamentation. The good agreement between our calculations and the angles measured experimentally consequently confirms that conical emission is

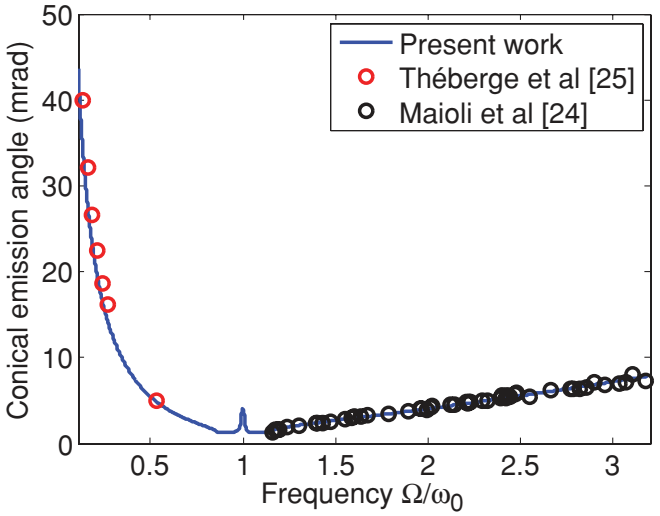

FIG. 2. (Color online) Comparison between experimental measurements of conical emission in the visible (black circle) and in the infrared (red square) with MI calculations (blue line).

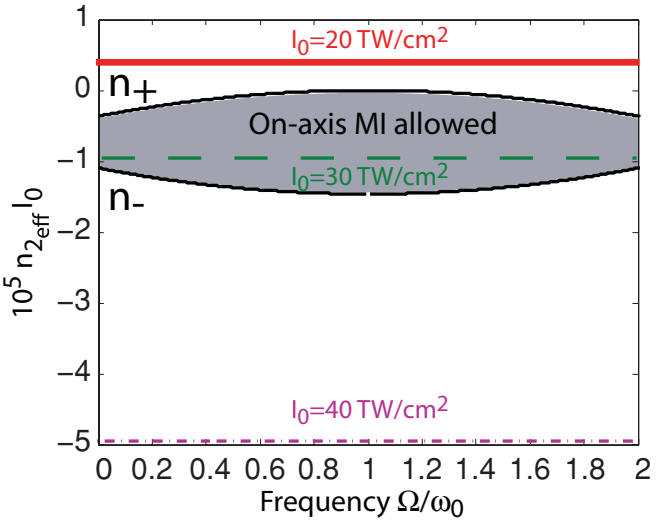

FIG. 3. (Color online) Diagram displaying the spectral region where on-axis MI occurs (gray region) and lying between n_+ and n_- (black lines). The lines display $n_{2_{\text{eff}}} I_0$ with $I_0 = 20$ TW/cm^2 (red solid line), 30 TW/cm^2 (dashed green line), and 40 TW/cm^2 (dash-dotted violet line), assuming the Kerr response as instantaneous, i.e., $n_{2_{\text{eff}}}(\omega) = n_{2_{\text{eff}}} \forall \omega$.

indeed generated by off-axis four waves mixing (4WM) during filamentation when $n_{2_{\text{eff}}} > 0$.

The situation significantly changes at higher intensity when $n_{2_{\text{eff}}} < 0$. In particular, the X pattern completely disappears, but a mechanism of MI still occurs. As stated earlier, MI occurs as soon as the condition $D_+(D_+ + N) + S^2/4 > 0$ is respected. This condition is equivalent to

$$n_- < n_{2_{\text{eff}}}(\omega) I_0 < n_+, \tag{9}$$

with

$$n_- = -\frac{k_0 D_+ \left(2 - \frac{k^{(1)^2}\omega^2}{2k_0^2}\right)}{k^{(1)^2}\omega^2},$$
$$n_+ = -\frac{D_+}{2k_0}.$$

More particularly, Fig. 3 displays the frequency range where on-axis ($k_\perp = 0$) MI is possible. When I_0 lies in the range 23.5–31.9 TW/cm^2, on-axis MI occurs. At higher intensity, $\forall\ (k_\perp, \omega)$, $n_{2_{\text{eff}}} I_0 < n_-$, meaning that no phase matching and, consequently, no MI can occur.

As a result, one can distinguish two cases. At moderate intensities [30 TW/cm^2; Figs. 1(c) and 1(d)] such that $n_- < n_{2_{\text{eff}}} I_0 < n_+$, strong on-axis MI is observed. For higher input intensities [40 TW/cm^2; Figs. 1(e) and 1(f)], the gain drastically decreases since the phase matching condition is no longer fulfilled.

One has to note that Théberge *et al.* [22] have observed on-axis infrared emissions which cannot be explained by off-axis 4WM processes. The MI calculations show that such on-axis emissions appear as soon as $n_{2_{\text{eff}}} < 0$.

One should emphasize that the general solution can be used to enhance or reduce the gain at specific frequencies by adjusting the phase and amplitude of the initial seeding. Figure 4 displays the MI gain bands for a pump intensity of 30 TW/cm^2 when $\widetilde{a}_0$ and $\widetilde{a}_0{}^\sharp$ are in phase (solid red line) and out of phase (dashed blue line). By adjusting their relative phases, the gain can be enhanced or reduced, the latter being maximal (minimal) when $\widetilde{a}_0$ and $\widetilde{a}_0{}^\sharp$ are in phase (out of phase).

We have shown previously that the higher order Kerr terms lead to on-axis MI in the normal dispersion regime. In this paragraph, we study the influence of self-steepening (SS) and space-time defocusing (STD) on MI band growth. The effect of these terms has already been discussed [23]. However, our general expression obtained in Sec. II allows us to better capture the MI dynamics. To perform this study, we have removed the contributions of these two terms (by setting $k^{(1)} = 0$) from the analytical and the numerical calculations, and we have repeated the same calculations as in the previous section. In Figs. 5(a) and 5(b), the intensity of the pump is 20 TW/cm^2 so that $n_{2_{\text{eff}}} > 0$. In that condition, neglecting both SS and STD does not lead to significant change of the

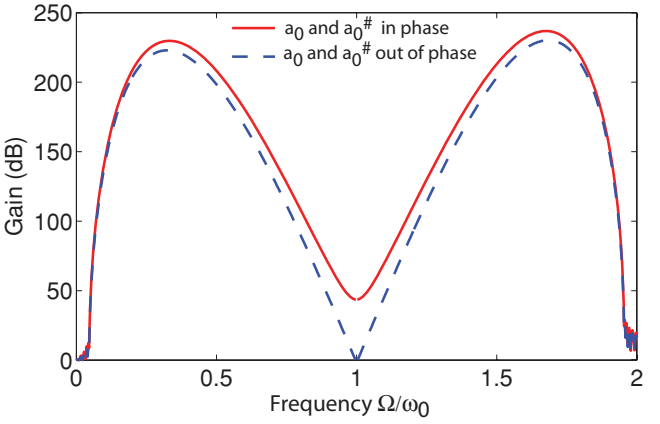

FIG. 4. (Color online) Gain bands through 1 m argon for a pump of 30 TW/cm^2 when $\widetilde{a}_0$ and $\widetilde{a}_0{}^\sharp$ are in phase (solid red line) and out of phase (dashed blue line).

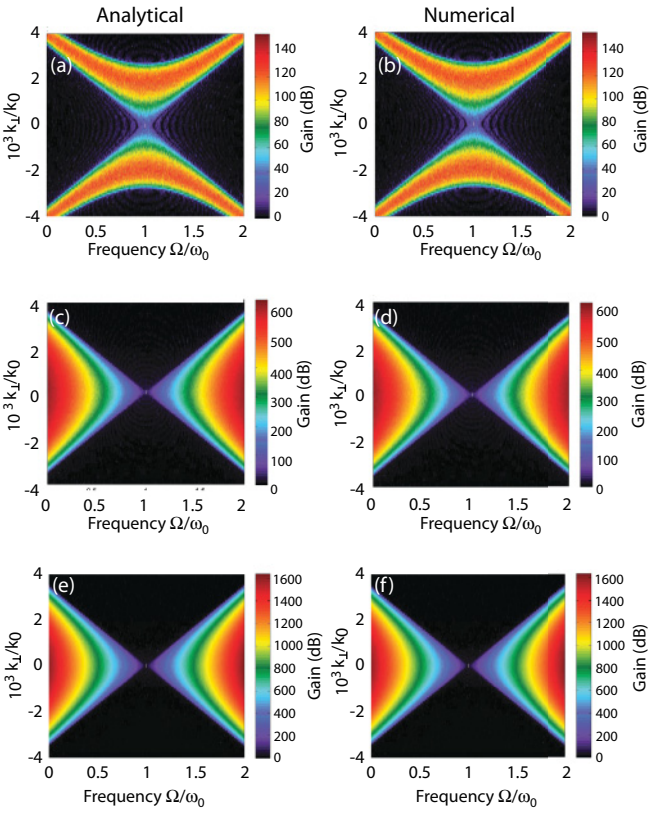

FIG. 5. (Color online) Comparison between numerical and analytical calculations of the gain (dB) in the $(k_\perp,\omega)$ space when neglecting both self-steepening and space-time defocusing. (a, b) Gain induced by a 20 TW/cm^2 pump ($n_{2_{\text{eff}}} > 0$), (c, d) gain induced by a 30 TW/cm^2 pump ($n_{2_{\text{eff}}} < 0$), and (e, f) gain induced by a 40 TW/cm^2 pump ($n_{2_{\text{eff}}} \ll 0$) after 1 m propagation.

MI bands. Only a slight deviation of the emission pattern can be noticed at frequencies far from the frequency pump. In the intermediate regime shown in Figs. 5(c) and 5(d), both shape and value of the gain change. In particular, neglecting SS and STD leads to a dramatic overestimation of the MI. This is due to the fact that the coupling between the pump and the MI bands is overestimated if one neglects SS and STD far from the frequency pump. Hence, without SS and STD, the maximal gain is obtained at $\omega = 0$ and $\omega = 2\omega_0$ while the full calculation gives the frequencies of maximal gain at $\omega = 0.3\omega_0$ and $\omega = 1.7\omega_0$ (see Fig. 4). At higher intensities [Figs. 5(e) and 5(f)], the MI gain bands are dramatically overestimated.

It results from Figs. 5(e) and 5(f) that neglecting both SS and STD suppresses the regime where MI is annihilated (high-intensity regime). When neglecting both SS and STD, the condition which has to be respected for the MI to occur is reduced to

$$n_{2_{\text{eff}}}(\omega) I_0 < n_+. \tag{10}$$

When the intensity increases, this condition is always respected, which leads to MI, as shown in Fig. 6.

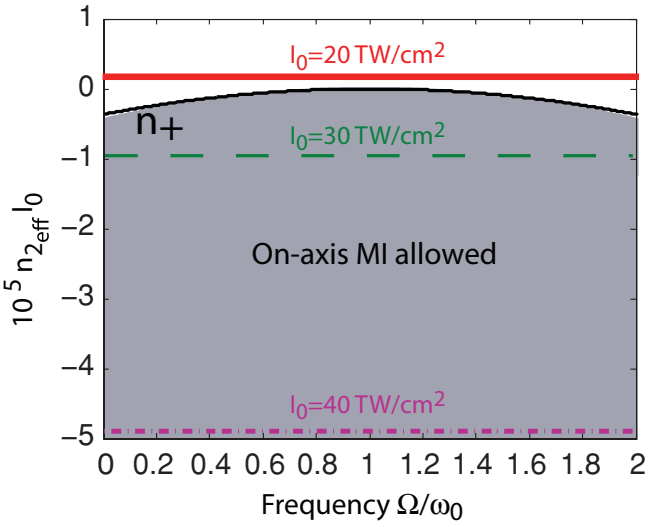

FIG. 6. (Color online) Diagram displaying the spectral region where on-axis MI occurs (gray region) when neglecting both SS and STD. This region is below n_+ (black line). The lines display $n_{2_{\text{eff}}} I_0$ with $I_0 = 20$ TW/cm^2 (red solid line), 30 TW/cm^2 (dashed green line), and 40 TW/cm^2 (dash-dotted violet line) assuming the Kerr response as instantaneous, i.e., $n_{2_{\text{eff}}}(\omega) = n_{2_{\text{eff}}} \forall \omega$.

B. 1-D analysis in the presence of Raman-induced delayed nonlinear response

In order to underline the generality of the solution derived in Sec. II, we calculated analytical and numerical solutions of the MI gain induced in a single mode fiber (SMF) in the presence of vibrational Raman nonlinearity. We considered the propagation of a 1550 nm 5 GW/cm^2 continuous wave in a 15-cm-long standard SMF (anomalous dispersion $k^{(2)} = -2.1 \times 10^{-26}$ s^2/m^1 and positive nonlinear index $n_2 = 2.6 \times 10^{-20}$ m^2/W^1) when the vibrational Raman effect is taken into account. Figure 7(a) displays both analytical and numerical MI-Raman gain bands. Since the general solution here takes into account the contributions of both real and imaginary parts of the Raman effect, the global gain is no more symmetric with respect to the pump frequency, with an amplification (absorption) at longer (shorter) wavelengths. We confirm again the excellent quantitative agreement between analytical and numerical results by showing in Fig. 7(b) that the relative error is less than 1%. The slight discrepancies are mainly from the finite propagation step used during the split-step Fourier numerical simulation. The combined action of parametric and Raman effects was already discussed in the early work of Bloembergen and Shen [24], and later, the resulting global (parametric-Raman) gain was widely investigated in the context of optical fibers [15,17,18,25]. With our general solution, the results obtained in these works can be retrieved only by calculating the parameter K. However, the gain evaluated with the help of an ansatz function [as shown in Fig. 7(a)] is only a rough estimation of the real gain, in particular, around the pump frequency. Moreover, calculating K cannot describe the asymmetry induced by the imaginary part of the Raman response function. When the MI gain bands do not overlap the Raman bands, positive gain is expected in the anti-Stokes band when simply evaluating K, while this part

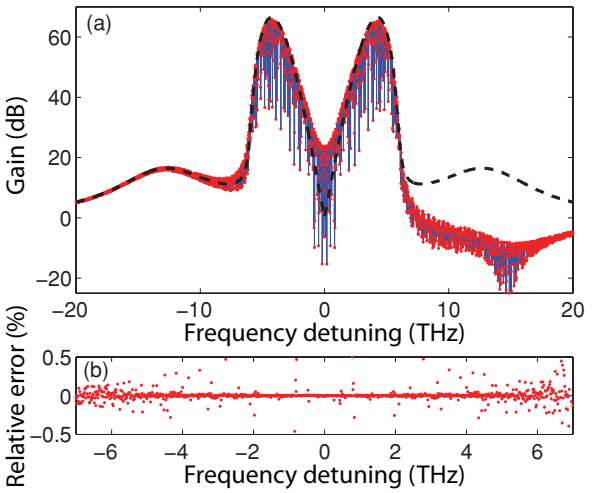

FIG. 7. (Color online) (a) Analytical (red dots) and numerical (solid blue line) MI gain bands calculated after 15 cm propagation in a SMF fiber with a pump of 5 GW/cm^2 in the presence of a delayed Raman nonlinearity. The black dashed line represents the gain calculated using an ansatz function. (b) Relative error between numerical and analytical calculations.

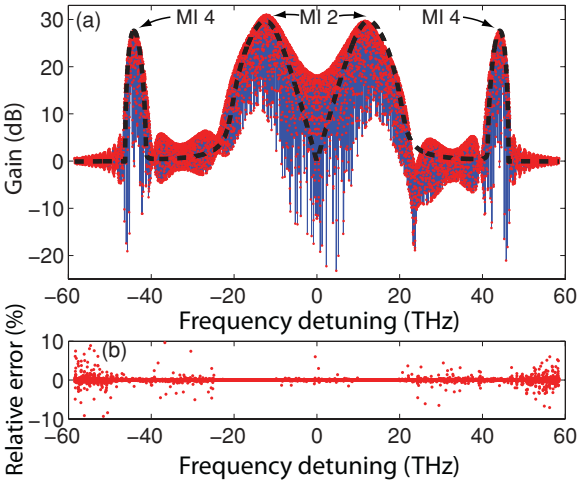

FIG. 8. (Color online) (a) Numerical (blue line) and analytical (red dots) MI gain bands obtained in 1-m-long PCF with two zero dispersion frequencies in presence of a delayed Raman nonlinearity. The black dashed line represents the gain calculated using an ansatz function. (b) Relative error between analytical and numerical calculations.

of the spectrum actually undergoes losses, as can be noticed in Fig. 7(a).

Nowadays, fiber dispersion properties can be engineered to a very high degree, thus allowing phase matching induced by higher order dispersion for ultrabroadband wavelength conversion [26]. For instance, the fourth-order dispersion can induce additional scalar MI bands in the normal dispersion regime [7]. It has been shown that in the presence of negative fourth-order dispersion near zero dispersion frequency, MI bands can grow up even by pumping in the normal dispersion regime. Consequently, by pumping in the anomalous dispersion regime, it is then possible to observe two pairs of MI sidebands [19]. We consider here this possible complex configuration of the MI process using the waveguide category of photonic crystal fibers (PCF). Figure 8 compares the analytical and numerical gain bands obtained by pumping a PCF which exhibits a low anomalous dispersion between its two zero dispersion wavelengths. Both linear and nonlinear fiber properties can be found in [27]. We used a 2.6 GW/cm^2 pump intensity at 1064 nm and a fiber length of 1 m. It clearly appears that Eq. (8) is also able to perfectly retrieve the two pairs of MI sidebands induced by second- and fourth-order dispersion terms. Besides the impact of higher order dispersion on the phase matching, our solution describes the asymmetrical shape of MI induced by the Raman gain. Indeed, we have adjusted here the input wave intensity so that the first standard MI sidebands are superposed to the silica Raman gain band (0–30 THz). Consequently, we retrieve again that the global MI-Raman gain is no more symmetric with respect to the pump frequency. As previously, the standard gain evaluation can give a rough estimation of the real gain in specific conditions.

C. Impact of Kerr electronic time response on the MI band growth

In this section, we underline the impact of the time response of the different higher order nonlinear Kerr terms on the induced MI. A recent work has highlighted the influence of a finite nonlinear response time [28] on the spatiotemporal MI growth, but using the usual simplified approach. Conversely, our method gives the exact solution even in the presence of a delayed nonlinear response without any approximation. Since the systematic study of any situation of MI is out of the scope of the present article, we have limited our work to 1-D MI gain in argon (as, for instance, relevant in the frame of hollow-core fiber propagation [29,30]) with non-purely-instantaneous nonlinear responses. Since no accurate information about the time response of the higher order nonlinearities is so far available, we used the same expression for all nonlinearities (i.e., the Debye-type relaxation model).

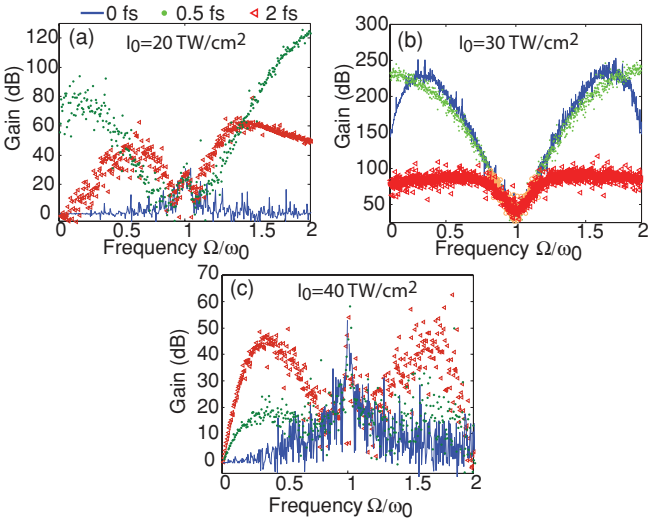

FIG. 9. (Color online) On-axis gain bands after 1 m propagation through argon with a pump of (a) 20 TW/cm^2, (b) 30 TW/cm^2, and (c) 40 TW/cm^2 with different Kerr electronic time responses (0 fs, blue line; 0.5 fs, green dots; and 2 fs, red triangles).

We write $\forall j$, $R_{2j}(t) = (1/\tau)e^{-t/\tau}$ for $t > 0$ and $R_{2j}(t) = 0$ for $t < 0$, although the different terms exhibit a priori distinct temporal behaviors. We used three distinct values of τ (0, 0.5 fs, and 2 fs) for pump intensities of 20, 30, and 40 TW/cm^2, which correspond to the three regimes observed when the Kerr effect is supposed to be instantaneous. Figure 9 displays the MI bands calculated after a 1 m propagation through 1 bar of argon with the same initial noise. In the low-intensity regime [Fig. 9(a)], while MI is not allowed for $\tau = 0$, on-axis MI is allowed for increasing τ. On the contrary, in the intermediate regime [Fig. 9(b)], a reduction by 20 orders of magnitude of the generated MI bands is observed when increasing the time response. Finally, in the high-intensity regime [Fig. 9(c)], increasing the time response leads to MI, while phase matching cannot be achieved if $\tau = 0$. It appears that even for very small values, the Kerr electronic time response is crucial to accurately describe the efficiency of MI band generation. In particular, we show that increasing the time response from 0 to 2 fs leads to a drastic change of the MI bands in all intensity regimes.

IV. CONCLUSION

In this article, we have derived the general expression of modulation instability in the presence of a continuous plane wave pump. The model, valid in 3-D, 2-D, and 1-D, allows us to evaluate the MI gain in the presence of higher order Kerr terms and any retarded nonlinear response (including the Raman response). We have shown that if the propagation of a pulse can be described by the equilibrium between the Kerr terms, then on-axis MI bands grow up as soon as the effective nonlinear index becomes negative. We have also highlighted the impact of self-steepening, space-time defocusing, andfinite-time nonlinear response on the MI band growth. Finally, in the frame of the fiber-propagation problem, we have shown that our analytical model perfectly describes the MI band growth in the presence of the Raman effect and complex dispersive properties. Moreover, we foresee that comparable analytical solutions can be found for vectorial MI, that is, for propagation through a birefringent medium.

ACKNOWLEDGMENTS

We gratefully acknowledge K. Hammani, P. Morin, and G. Millot for very fruitful discussions. This work was supported by the ANR COMOC (Grant No. ANR-07-BLAN-0152-01) and by the FASTQUAST ITN Program of the seventh FP. B.K. acknowledges support from the French Agence Nationale de la Recherche project MANUREVA (Grant No. ANR-08-SYSC-019) and from the Conseil Régional de Bourgogne.

[1] V. I. Bespalov and V. I. Talanov, Zh. Eksp. Teor. Fiz.-Pis'ma Red. **3**, 471 (1966) [JETP Lett. **3**, 307 (1966)].
[2] T. B. Benjamin and J. E. Feir, J. Fluid Mech. **27**, 417 (1967).
[3] K. Tai, A. Hasegawa, and A. Tomita, Phys. Rev. Lett. **56**, 135 (1986).
[4] D. Kip, M. Soljacic, M. Segev, E. Eugenieva, and D. N. Christodoulides, Science **290**, 495 (2000).
[5] V. E. Zakharov and L. A. Ostrovsky, Physica D **238**, 540 (2009).
[6] J. M. Dudley, G. Genty, F. Dias, B. Kibler, and N. Akhmediev, Opt. Express **17**, 21497 (2009).
[7] S. Pitois and G. Millot, Opt. Commun. **226**, 415 (2003).
[8] F. Biancalana and D. V. Skryabin, J. Opt. A: Pure Appl. Opt. **6**, 301 (2004).
[9] F. Vidal and T. W. Johnston, Phys. Rev. Lett. **77**, 1282 (1996).
[10] V. Loriot, E. Hertz, O. Faucher, and B. Lavorel, Opt. Express **17**, 13429 (2009); **18**, 3011(E) (2010).
[11] P. Béjot, J. Kasparian, S. Henin, V. Loriot, T. Vieillard, E. Hertz, O. Faucher, B. Lavorel, and J.-P. Wolf, Phys. Rev. Lett. **104**, 103903 (2010).
[12] J.-L. Oudar, J. Quant. Electron. **19**, 713 (1983).
[13] Q. Lin and G. P. Agrawal, Opt. Lett. **31**(21), 3086 (2006).
[14] T. Brabec and F. Krausz, Phys. Rev. Lett. **78**, 3282 (1997).
[15] S. Trillo and S. Wabnitz, J. Opt. Soc. Am. B **9**, 1061 (1992).
[16] J. E. Rothenberg, Phys. Rev. A **42**, 682 (1990).
[17] K. J. Blow and D. Wood, IEEE J. Quantum Electron. **25**, 2665 (1989).
[18] E. A. Golovchenko and A. D. Pilipetskii, J. Opt. Soc. Am. B **11**, 92 (1994).
[19] F. Biancalana, D. V. Skryabin, and P. St. J. Russell, Phys. Rev. E **68**, 046603 (2003).
[20] D. R. Solli, C. Ropers, P. Koonath, and B. Jalali, Nature (London) **450**, 1054 (2007).
[21] P. Maioli, R. Salamé, N. Lascoux, E. Salmon, P. Béjot, J. Kasparian, and J.-P. Wolf, Opt. Express **17**, 4726 (2009).
[22] F. Théberge, M. Chateauneuf, V. Ross, P. Mathieu, and J. Dubois, Opt. Lett. **33**, 2515 (2008).
[23] S. Wena, W. Hua, H. Guoa, and D. Fan, Opt. Commun. **202**, 339 (2002).
[24] N. Bloembergen and Y. R. Shen, Phys. Rev. Lett. **12**, 504 (1964).
[25] M. J. Potasek, Opt. Lett. **12**, 921 (1987).
[26] P. St. J. Russell, J. Lightwave Technol. **24**, 4729 (2006).
[27] B. Barviau, B. Kibler, A. Kudlinski, A. Mussot, G. Millot, and A. Picozzi, Opt. Express **17**, 7392 (2009).
[28] L. Zhang, S. Wen, X. Fu, J. Deng, J. Zhang, and D. Fan, Opt. Commun. **283**, 2251 (2010).
[29] P. Béjot, B. E. Schmidt, J. Kasparian, J.-P. Wolf, and F. Legaré, Phys. Rev. A **81**, 063828 (2010).
[30] B. E. Schmidt *et al.*, Appl. Phys. Lett. **96**, 121109 (2010).